National Research University Higher School of Economics

Faculty of Computer Science

HSE and University of London Double
Degree Programme in Data Science and
Business Analytics

BACHELOR'S THESIS

Research Project

Deep Learning Neural Networks to Identify Phlebology Disease (Joint Project with Antireflux Hospital)

Prepared by the student of Group 192, Year 4,

Rutsinskiy Arsenty

Thesis Supervisor:

Deputy Head of Department, Ph.D. Gromov Vasilii

Moscow

2023

Abstract

Phlebology is a medical specialty concerned with the diagnosis and treatment of cardiovascular disorders. The identification and classification of such diseases is challenging due to the complex anatomical and physiological structure of the venous system. In recent years, deep learning neural networks have emerged as a promising tool for medical image analysis. This paper proposes a neural network approach to identify and classify phlebology diseases using medical images (MRI scans), provided by “Antireflux” medical center. The main problem is developing a neural network architecture which can achieve good results for medical purposes having a small and imbalanced dataset. A generative adversarial network (GAN) architecture using physics-informed neural network (PINN) paradigm is proposed as a solution and a main topic of the research. Different combinations of deep learning tools have been applied to test the results and find the most accurate approach. The results of the study indicate that deep learning neural networks can be a valuable tool for phlebology disease diagnosis and classification, providing an efficient and non-invasive alternative to traditional diagnostic methods.

Key words: Convolutional neural networks, Generative-adversarial networks, Physics-informed neural networks, Phlebology, Cardiovascular system, Human hemodynamics, Data augmentation

Аннотация

Флебология — это медицинский раздел, занимающийся изучением и диагностикой сердечно-сосудистых заболеваний. Идентификация и классификация таких заболеваний является довольно проблематичной задачей из-за сложной анатомической и физиологической структуры венозной системы. В последние годы нейронные сети глубокого обучения стали перспективным инструментом для анализа медицинских изображений. В данной работе предлагается нейросетевой подход для идентификации и классификации флебологических заболеваний с использованием медицинских изображений (снимков МРТ), предоставленных медицинским центром "Антирефлюкс". Основная проблема заключается в разработке архитектуры нейронной сети, которая сможет достичь приемлемых результатов для медицинских целей на небольшом и несбалансированном наборе данных. В качестве решения и основной тематики исследования предлагается архитектура генеративной состязательной сети (GAN), использующая парадигму физически-информированной нейронной сети (PINN). Для оценки результатов и поиска наиболее точного подхода были применены различные комбинации инструментов глубокого обучения. Результаты исследования показывают, что нейронные сети глубокого обучения могут быть ценным инструментом для диагностики и классификации флебологических заболеваний, предоставляя эффективную и неинвазивную альтернативу традиционным методам диагностики.

Ключевые слова: Сверточные нейронные сети, Генеративно-состязательные сети, Физически-информированные нейронные сети, Флебология, Сердечно-сосудистая система, Гемодинамика, Аугментация данных

Table of Contents

Introduction

Recent article published by the World Health Organization (WHO) states that nearly a third of all deaths on the planet are caused by cardiovascular diseases [1], meaning that every two seconds heart or vascular pathologies lead to one more death. In Russia the situation is even more critical: such diseases kill 900,000 people a year, which is a little less than half of all deaths in the country [2].

The situation got even worse with the COVID-19 pandemic. An increased workload of medical staff led to less attention than usual for patients with cardiovascular diseases, and patients themselves were wary of visiting clinics due to the high probability of contracting the coronavirus. Introduction of the self-isolation regime has entailed people's physical activity decrease, diet change, and stress levels increase, all of which only increased people's exposure to heart or vascular pathologies.

It is possible to prevent most of the diseases and reduce the likelihood of serious complications by detecting the disease in time and prescribing appropriate treatment. Phlebologists currently have at their disposal a wide range of modern methods for examination of patients. The most effective one is a magnetic resonance imaging (MRI). This is a non-invasive safe method, which gives an opportunity to assess the condition of the patient's cardiovascular system and to reveal pathology in advance. However, it takes one to three hours to interpret an MRI scan, depending on its complexity. Given the growing volume of medical examinations, the problem of reducing the analysis time and making a correct diagnosis is critical.

In order to exclude the possibility of medical errors and increase the capacity of diagnostic centers, scientists suggest using mathematical models that will help to automate the analysis of many tomographic images and search for certain pathologies. The most promising direction is an approach based on deep neural networks, which are capable for self-training based on provided data. The development of neural network models for diagnostics and classification of diseases of the circulatory system is both of research and practical interests, and it is aimed at creating clinical decision support system (CDSS) as a helpful tool for vascular specialists.

Tasks statement

The purpose of this paper is to develop deep learning neural networks for an effective identification of cardiovascular diseases. To achieve the goal the following steps are required:

- Review of works on phlebology disease identification;
- Explore and preprocess provided data;
- Study the cardiovascular system and human hemodynamics;
- Develop deep learning neural network for disease identification models based on MRI images and PINN paradigm;
- Carry out experimental studies of the effectiveness of the proposed methods.

Understanding the workings of the human cardiovascular system and related hemodynamics models is fundamental to the creation of a deep learning neural network purposed for phlebology disease detection. This knowledge allows us to create a model that reliably reflects the complex physiological processes of the human cardiovascular system, a key factor in interpreting the outcomes generated by the neural network. The differential equations associated with the cardiovascular system model are integral to describe the connections between various physiological parameters like blood flow, pressure, and resistance. These equations lay the groundwork for the creation of a mathematical model that effectively captures the dynamics of the cardiovascular system. Such a model is vital for training our deep learning neural network. Additionally, we cannot overlook the importance of data exploration and preprocessing in the development of a reliable deep learning neural network. The data set aside for training the neural network needs to be thoroughly examined and analyzed to identify an effective approach. It may be necessary to undertake preprocessing measures to guarantee the data is fit for training the neural network in the most sensible manner. When it comes to deploying a deep learning neural network, the process entails creating and training a model that can reliably identify phlebology disease from the given data. This phase includes the selection of suitable neural network architectures, defining hyperparameters, and training the model utilizing the preprocessed data. Once trained, the model can predict the likelihood of phlebology disease in new patients.

Chapter 1. A neural network approach for the diagnosis of cardiovascular diseases

Pathology of the lower limbs veins in the modern world is one of the most common diseases of civilization, therefore early diagnosis and monitoring of the dynamics of chronic vein diseases are the priority tasks of modern medicine. For many years, the most mass instrumental method of medical diagnostics, especially in case of suspected deep vein thrombosis, was phlebography. The main disadvantages of this radiological method are its invasiveness, the risk of allergic reactions to the injected X-ray contrast agent, radiation exposure of the patient and medical staff.

Active interest in studying the possibilities of applying artificial neural networks for the analysis of cardiovascular pathologies has started at the beginning of the last decade and continues up to nowadays. Thus, the work [3] proposes the AI-based solution for congenital heart disease (CHD), which is an echocardiogram video-based binary classification model that judges whether echocardiogram videos contain heart defects, the authors of the study [4] performed comparative analysis of different ML techniques, such as gradient boosting, recurrent neural networks (RNNs) and reinforcement learning (RL), in monitoring cardiovascular patients and highlighted the interpretability of the AI decisions and generalizability issues. Prospects for future research and value of applying artificial neural networks in medicine are discussed in [5, 6, 7]. It is noted that in many tasks neural networks are much more effective than other mathematical algorithms. The key role in this success is played by neural networks' ability to learn, which allows them to identify complex dependencies in data and achieve generalizations. Another important advantage of neural network approach is the possibility of effective paralleling algorithms, that allows to significantly increase computation performance with the use of graphics processors. The availability of powerful computational resources and open-source libraries has contributed to an increase in the number of studies devoted to the possibilities of clinical use of deep learning techniques in recent years, especially in medical images analysis. Quite detailed review and practical guideline on this topic can be found, for instance in [8, 9].

1.1 Neural network architectures and medical data

There are dozens of various neural network architectures, which are widely used in different fields including medicine. Examples of such architectures are shown in the picture below. In the medical sector in particular, most of the developments have been achieved using Convolutional Neural Networks (CNNs).

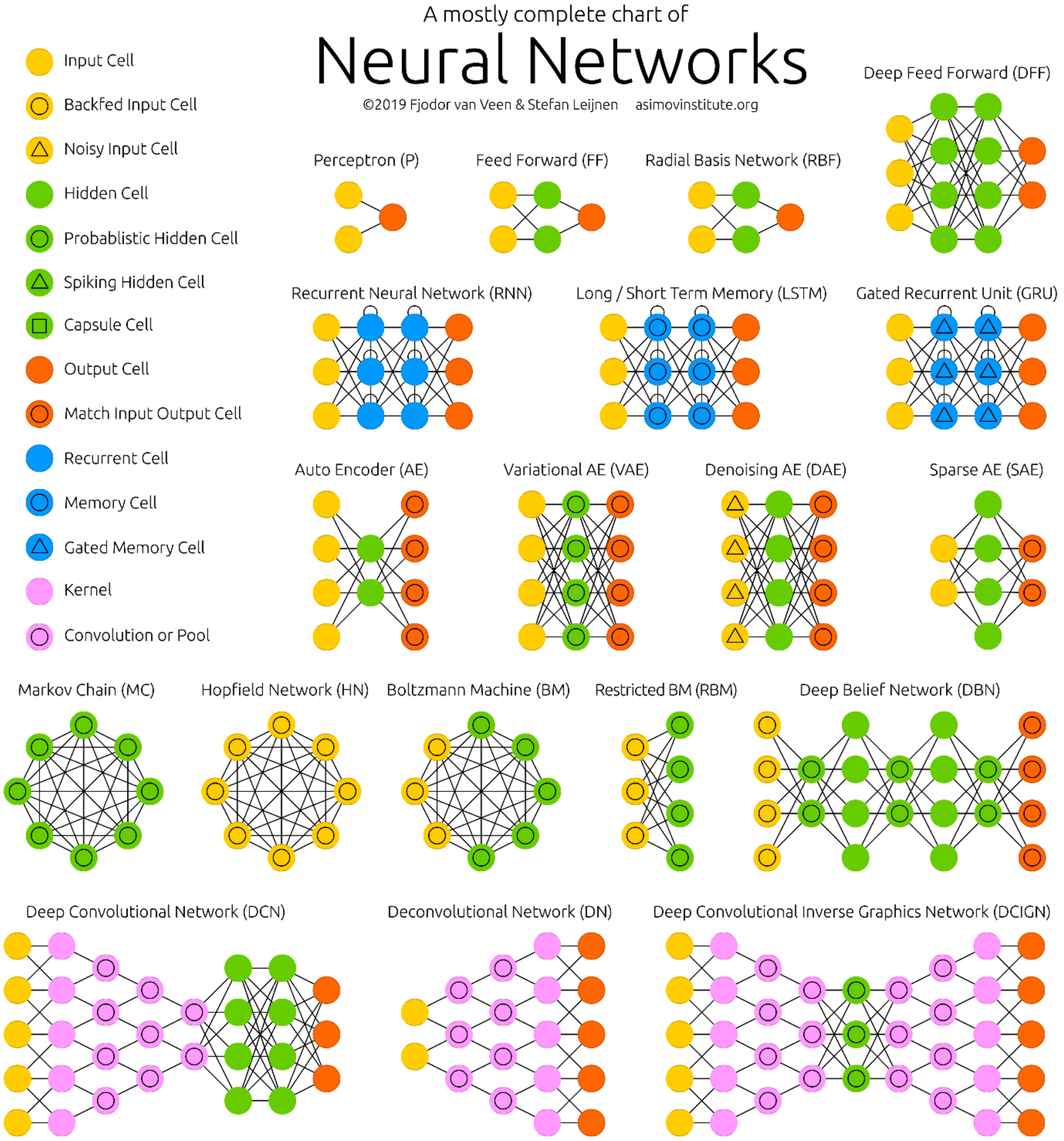

Figure 1. Neural network architectures

Examples of such architectures are shown in the picture below. In the medical sector in particular, most of the developments have been achieved using Convolutional Neural Networks (CNNs) [26].

1.1.1 Convolutional Neural Networks

The working process of convolutional neural networks are inspired by the principle of biological neural structure in pattern recognition. They are often used to recognize objects in photos, classify images and audio signals, and are also actively used in medicine, including diagnostics based on MRI scans. Figure 2 shows an example of such a neural network.

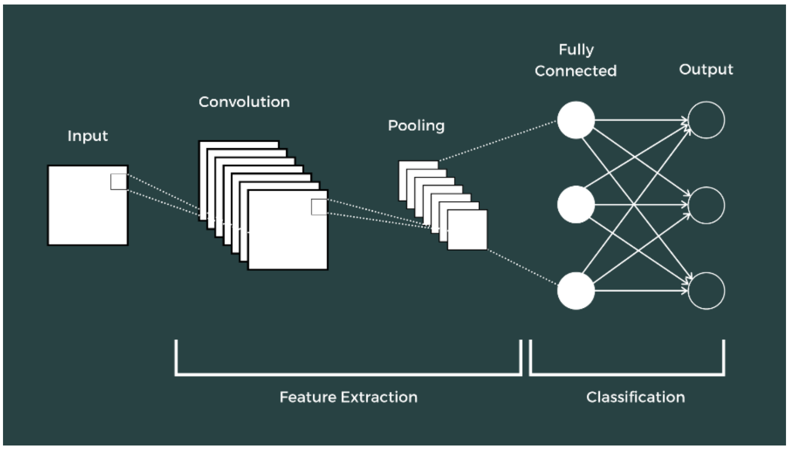

Figure 2.Convolutional neural network principle

When constructing convolutional networks, the standard technique consists of multiple alternation of convolutional and pooling layers and the subsequent addition of several fully connected layers, the last of which eventually yields the probability of an object belonging to each class in the classification problems.

The convolutional layer takes as input a matrix of size a×b×c derived from the input image where the first two parameters are the size of the image, and the last takes values of RGB channels (from 0 to 255). Then the convolution operation takes place, an example of which is shown in Figure 3: the image passes through a convolution kernel of some given size, each pixel is element by element multiplied by the corresponding weight in the matrix, the results are summed and recorded as the corresponding pixel in the next image.

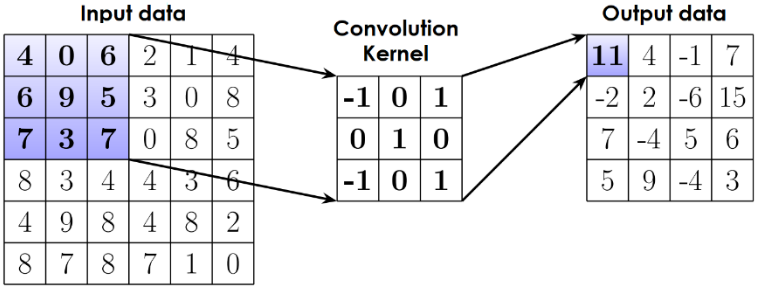

4	**0**	**6**	2	1	4
6	**9**	**5**	3	0	8
7	**3**	**7**	0	8	5
8	3	4	4	3	6
4	9	8	4	8	2
8	7	8	7	1	0

-1	**0**	**1**
0	**1**	**0**
-1	**0**	**1**

11	4	-1	7
-2	2	-6	15
7	-4	5	6
5	9	-4	3

Figure 3. Convolution process

After each convolutional layer an activation function can be applied. Usually, it is Sigmoid $f(x) = \frac{1}{1+e^{-x}}$, ReLU $f(x) = \max(0, x)$ or Tanh $f(x) = \frac{e^{x}-e^{-x}}{e^{x}+e^{-x}}$.

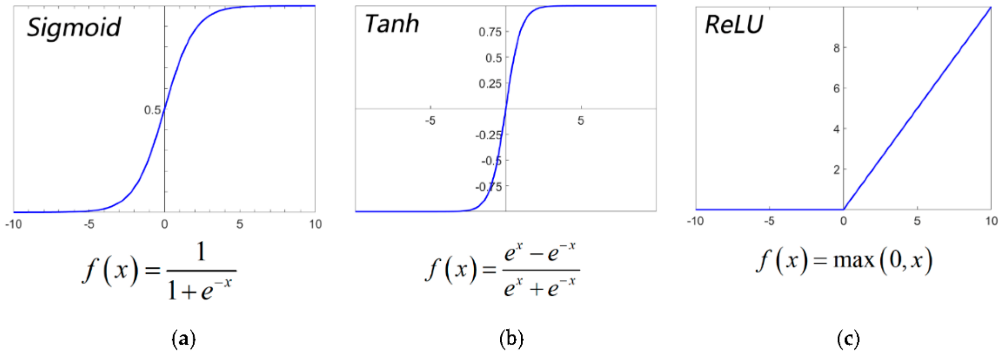

Figure 4. Activation functions

Then the image passes through pooling layer, which significantly decreases spatial dimension of input. It meets two key objectives. The first is to reduce parameters or weights, lowering the computational cost. The second is to prevent the network from becoming overfit. Only relevant data should be extracted, and useless data should be discarded through a perfect pooling process.

Convolutional neural networks have a large set of hyperparameters: in particular, the number and types of layers and cores in each of them, activation functions of layers, steps of filter shift; as well as variable parameters borrowed from fully connected neural networks: structure of fully connected layers, learning rate, learning stopping criterion, etc. There are no clear rules for the selection of the values of these parameters, but in most cases, they can be selected intuitively, depending on the needs of a particular task.

1.1.2 Medical data related problems

The quality of initial data is of great importance when training any neural network. Medical data is a lot more problematic than any other. There are a number of strict requirements to it, such as suitability for machine processing, sufficient number of measurements, physical correctness, compatibility. In addition, taking into account legal constraints as well as ethical considerations, it is quite difficult to obtain a large set of patient data: all data must be preprocessed - any information that may violate patient anonymity must be excluded from consideration in order to maintain medical confidentiality [23].

The problem of limited input dataset and its imbalance often arises in various tasks related to image recognition and processing, but it is especially relevant in medical research [24]. Thus, an example is the article, where the authors faced the problem of the small size of the original dataset, which did not allow them to achieve a higher classification reliability until they introduced developed preprocessing technique [25].

Therefore, the smaller the initial data, the worse the neural network will work in real conditions. Training on a small dataset could lead to model overfitting, when the classification accuracy on the training sample is close to 100%, however the result on new samples is poor. The improvement of generalizability, or the difference in the quality of the model's performance on the already viewed data in comparison with the data it has not encountered before, of such a model with restricted in terms of size initial dataset is a difficult task, which can be solved by means of data augmentation.

1.1.3 Data augmentation algorithms

Data augmentation is the extension of a dataset based on existing samples. There are several basic ways to augment data, including adding noise, cropping, flipping, rotation, scaling, shifting, brightness and contrast change.

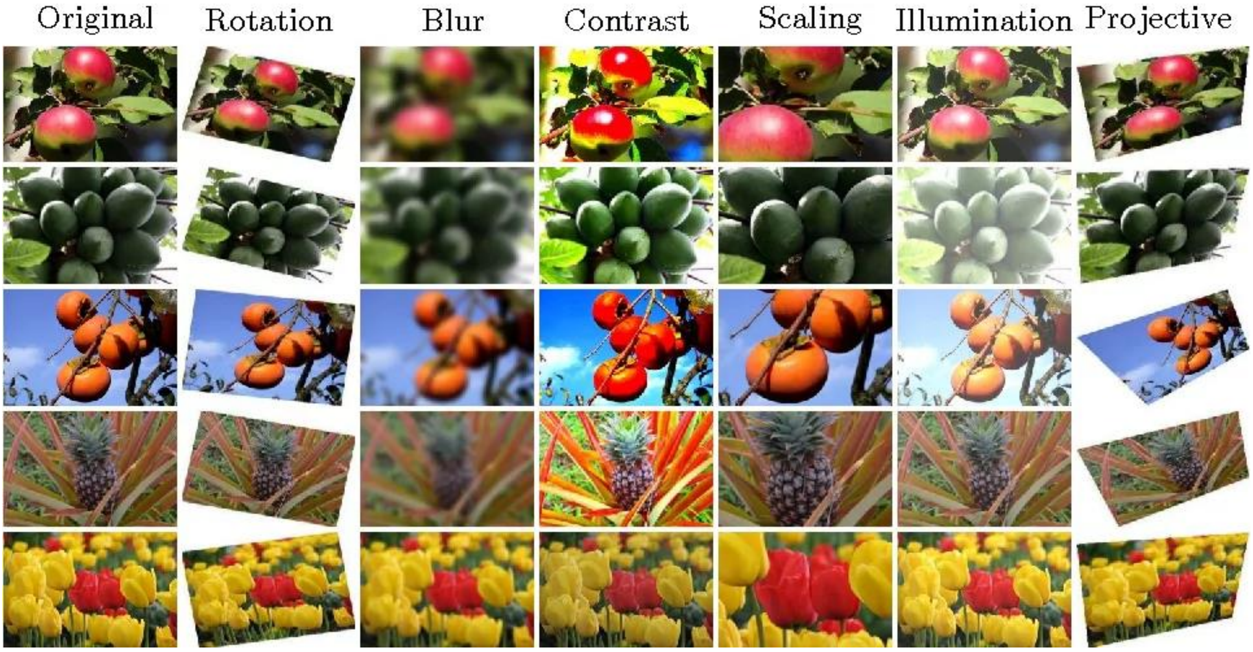

Figure 5. Standard data augmentation methods

Growing popularity of the topic of image recognition and classification led to creation of many data augmentation tools. For example, the cutting-splicing data augmentation (CS-DA) method has been developed, which offers more advanced augmentation methods besides the standard ones [12]. It augments the dataset by splicing different position components cut from different original medical images into a new image (Figure 6).

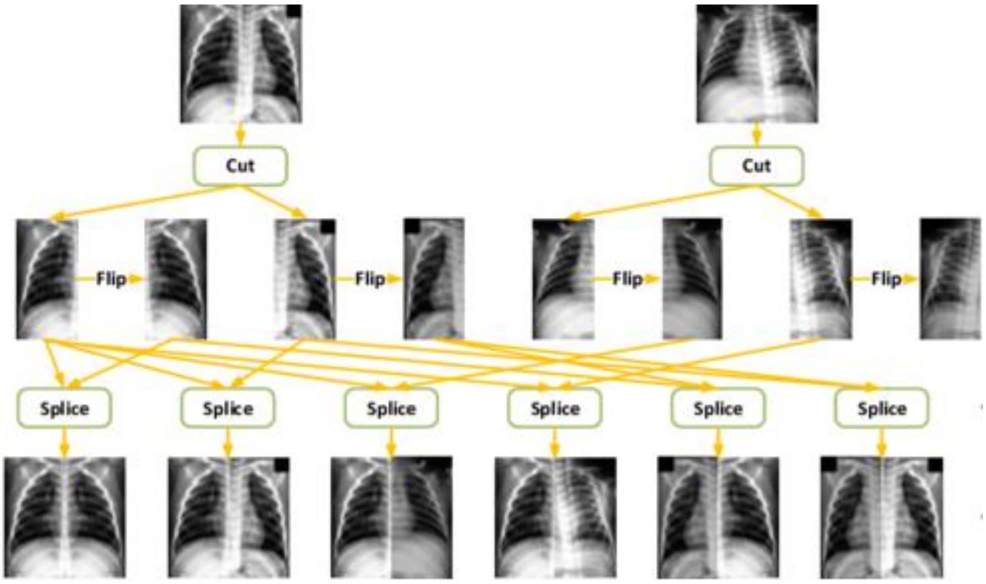

Figure 6. Cutting-splicing data augmentation method

Augmentation techniques depend on the specific task. However, when working with medical images, the benefit of using standard augmentation methods is not so significant. Firstly, no fundamentally new images appear in the set [12], and secondly, medical images adhere to strict standards. Thus, MRI images are centered, vertically and horizontally aligned, and normalized for brightness and contrast. This severely limits the possibilities of expanding the original dataset and prompts a more advanced way of increasing the dataset, namely, generation of images using generative-adversarial network (GAN).

1.1.4 Generative-adversarial networks (GAN)

The use of generative adversarial networks, or GANs, allows to obtain new images on the basis of existing ones. The principle of such a network is shown in Figure 7.

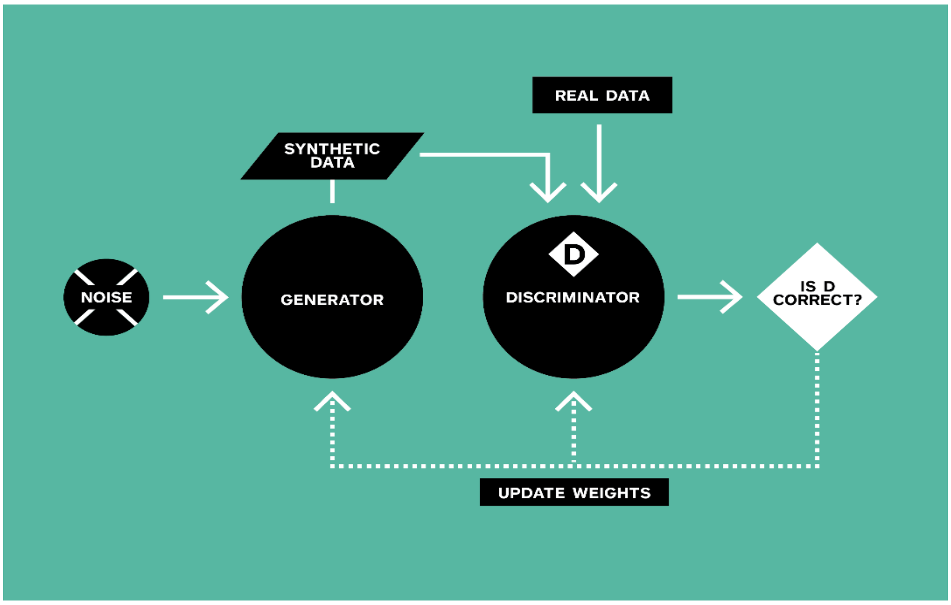

Figure 7. The principle of the Generative Adversarial Network

The network consists of two parts: a generator and a discriminator. Generator G randomly generates images from a noise vector and sends them for processing to discriminator D, which, in turn, tries to distinguish the real image from the generated one. After a certain number of iterations, the images provided by the generator become indistinguishable from the real images from the original dataset, resulting in a significant increase in the number of available samples.

A successful example of using GAN to generate a large set of synthetic MRI brain images is the work done by Armanious et al. in 2019. They developed a GAN-based method called "MedGAN" to generate synthetic brain MRI scans [13]. MedGAN builds upon recent advances in the field of generative adversarial networks (GANs) by merging the adversarial framework with a new combination of non-adversarial losses.

The evaluation of their approach showed promising results. The models trained on the augmented dataset, which included both real and synthetic scans, outperformed the models trained only on the original real dataset. The augmentation with synthetic scans helped improve the generalization of the models and their ability to classify brain tumors accurately.

1.2 Physics-informed neural network (PINN) paradigm

The availability of a large number of initial samples makes a process of model training a lot easier. Nonetheless, existing models still have too low accuracy to be used for real life problems. To improve the classification accuracy, it is suggested to use more complex neural network architecture or fundamentally new approaches. An example of such an approach is the use of the PINN paradigm, which allows to embed knowledge about physical laws in a neural network. This is accomplished by adding uncertainties to the loss function, which are calculated on the basis of physical laws and set the degree of "physical implausibility" of the model. With this approach the model adjusts to physical processes and produces physically correct results. When the error propagates backwards, the model minimizes the value of the loss function, which means that every invariance approaches zero and the physical equation becomes physically correct. When applied to the study of phlebology problems, the basic laws of hemodynamics are used as physical laws for the PINN paradigm.

Thus, an example of applying PINN for hemodynamic predictions using medical imaging is demonstrated at the paper done by Sarabian et al. in 2022 [14]. In this study the authors present a physics-based deep learning framework to produce physically consistent brain hemodynamic parameters with high spatiotemporal accuracy by combining sparse clinical observations with one-dimensional (1D) reduced-order model (ROM) simulations. Their deep learning network creates high-resolution maps of velocity, area, and pressure in the entire brain vasculature using in vivo real-time Transcranial Doppler (TCD) velocity measurements at various points in the brain along with baseline vessel cross-sectional areas obtained from 3D angiography pictures. Then, using related sparse velocity measurements, the authors accurately forecast the changes in vasospastic local artery diameters to demonstrate the clinical importance of this technique in detecting cerebral vasospasm (CVS). By creating synthetic blood flow data after cerebral vasospasm at different levels of stenosis, they demonstrate this capability. This work shows that physics-based deep learning can estimate and quantify subject-specific cerebral hemodynamic variables with high accuracy even in the absence of knowledge of inlet and outlet boundary conditions, which is a significant limitation for the accuracy of the conventional purely physics-based models.

1.2.1 Cardiovascular system

A closed human circulatory system or any selected part of it is represented as a graph consisting of edges and vertices (Fig. 8).

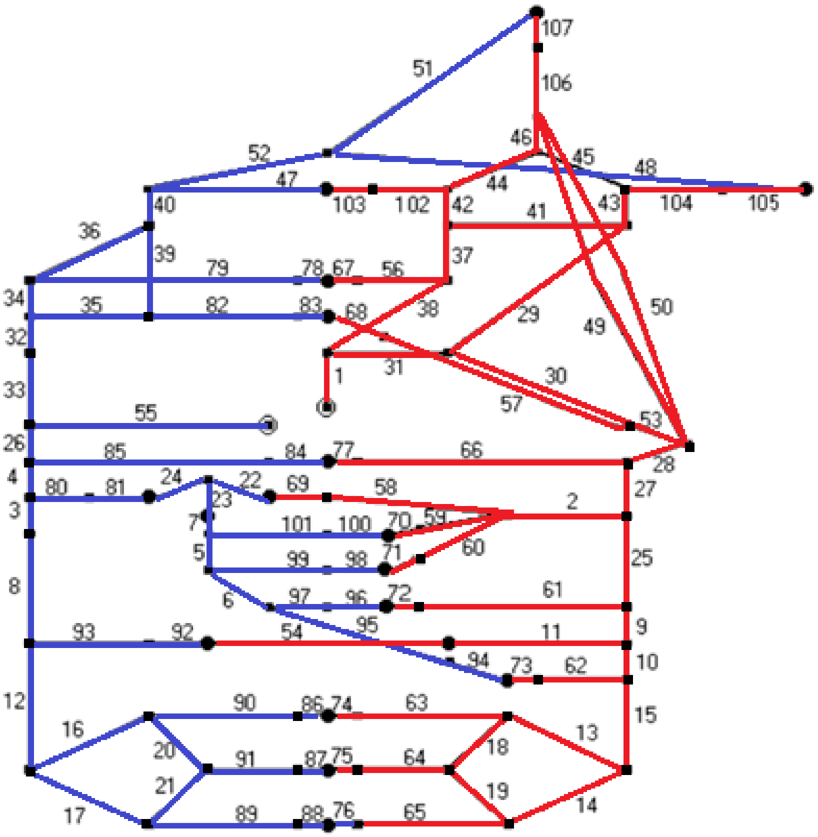

Figure 8. Cardiovascular system graph

Vessels of the arterial part are highlighted in red, and vessels of the venous part of the human great circle of circulation are highlighted in blue [15]. Individual capillaries or blood vessels are represented by the graph's ribs, while functional characteristics of either branching blood vessels regions, muscular tissues, or organs are assigned to the graph's vertex nodes. The area where two or more vessels converge is called a bifurcation point. Vessels are considered to be sufficiently extended compared to their diameter. This assumption allows to use for mathematical description of the process of blood flow in blood vessels an approximation based on the laws of fluid flow in tubes with elastic walls.

1.2.2 Human hemodynamics

The modern approach to the evaluation of the cardiovascular system is based on the understanding of blood flow patterns. The dynamics of the circulatory system are simulated using a variety of mathematical models. Quasi-dimensional modelling approach is currently the most frequently used method in such studies [16]. They allow to consider in detail local processes in individual vessels taking into account the whole blood circulation system of a human.

The law of conservation of mass, the law of conservation of momentum, and the equation characterizing the bifurcation point, which combines pressure and vessel cross-sectional area, are typically used to define a quasi-uniform model. While the first two equations apply to all vessels, the third equation takes into consideration all of a given vessel's local specifics [17].

Law of conservation of mass

At the bifurcation point the law of conservation of mass is used:

$$S_1 v_1 \ = \ S_2 v_2 \ + \ S_3 v_3,$$

where S – cross-sectional area, v – blood flow rate.

Navier-Stokes equations

The Navier-Stokes equations are usually used to describe a viscous Newtonian fluid. In the case of an incompressible fluid:

$$\frac{\partial S}{\partial t} + \frac{\partial (Sv)}{\partial x} = const,$$

$$\frac{\partial v}{\partial t} + \frac{\partial (\frac{v^2}{2} + \frac{p}{\rho})}{\partial x} = const,$$

where S – cross-sectional area, v – blood flow rate, p – vessel pressure, ρ – density.

The first equation describes the law of continuity and the second - the law of conservation of momentum.

Bernoulli's equation

The law of conservation of energy describing the parameters of a particular vessel is a Bernoulli's law, which states that the value remains constant along the line of current motion.

$$\rho\frac{v^2}{2} + \rho * g * h + p = const$$

where ρ – density (blood), v – blood flow rate, h - height, p – vessel pressure, g – gravitational acceleration.

1.3 Chapter results

This chapter reviewed the existing approaches to the diagnosis of phlebology diseases using neural networks of different architectures. The problem of collecting and using medical data was revealed, as well as the ways to solve it, in particular - artificial expansion of initial data sets using basic augmentation methods and generative-adversarial networks. In addition, mathematical and physical approaches to blood flow modeling were studied.

Based on the results of this study, a decision of preferred methods was made to solve the tasks set in this paper, namely the use of generative-adversarial networks, which have proved effectiveness in related fields of medicine, in combination with the recently proposed PINN paradigm. These methods will be discussed in more detail in the next chapter.

Chapter 2. Model development and data preprocessing

2.1 Dataset description

Model training was performed using a dataset provided by the Antireflux Phlebology Center. The dataset contains 810 images: 10 MRI images of the pelvic region of 81 patients each. Patients were diagnosed according to the CEAP classification system [18]. According to this classification, chronic vein diseases can be divided into seven clinical classes from C0 to C6 with specific objective signs:

- C0 No visible or palpable signs of venous disease,
- C1 Telangiectasis or reticular veins,
- C2 Varicose veins; distinguished from reticular veins by a diameter of 3mm or more,
- C3 Edema,
- C4 Changes in skin and subcutaneous tissue secondary to CVD,
- C5 Healed venous ulcer,
- C6 Active venous ulcer.

In this paper, a patient who is assigned a clinical class of C0 to C2 is considered healthy, otherwise considered sick.

2.2 Image preprocessing

Initially, all images had a resolution of 512x512 pixels, but to reduce their size and, consequently, the complexity of the calculations, the low-informative edges were cropped to a size of 300x300 (Fig. 9):

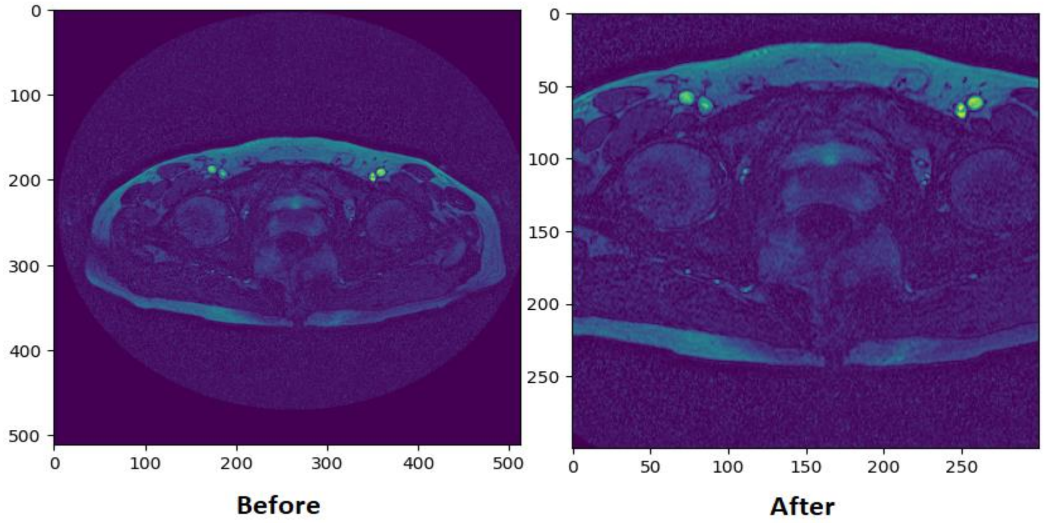

Figure 9. MRI images before and after cropping

Then, for each patient, all 10 images were merged into a single 3000x300 image to fit in the model. The dataset was divided into 21 test samples and 60 training samples, 16 and 43 images of which represent healthy patients respectively. The data was preprocessed to fit TensorFlow architecture, shuffled and organized into the batches to improve training performance and prevent any biases during model training.

The problem of the dataset being small and unbalanced led to the decision to make the generation of MRI samples for sick patients as the key objective for generator. It was achieved by ensuring that the discriminator identifies original MRI images of only sick patient as original ones, but original images of healthy patients as well as any other generated images as generated.

2.3 Cardiovascular graph description

To use the PINN paradigm, it is necessary to define a graph of the human circulatory system using the above-mentioned physical laws. Of the complete graph above (Fig. 8) we are interested only in a small part, in which only three small circuits of blood circulation are involved from the vessels of interest that pass through the legs and liver (Fig. 10). It consists of 12 bifurcation points and 16 edges (vessels).

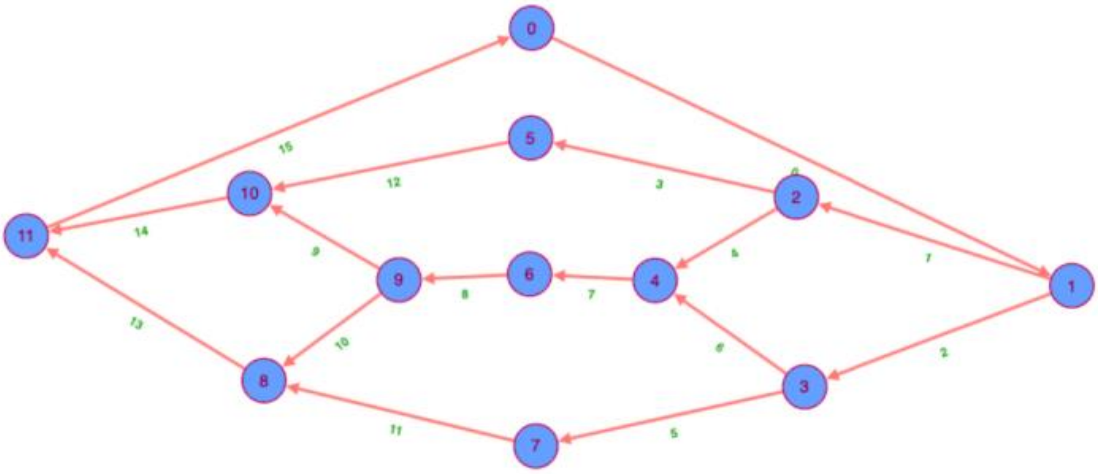

Figure 10. Simplified cardiovascular system graph

It is possible to describe the vessels at the bifurcation points using the equations of hemodynamics (the law of conservation of mass and constancy of the Bernoulli integral). An example of vessel bifurcation points is shown in Figure 11 [19].

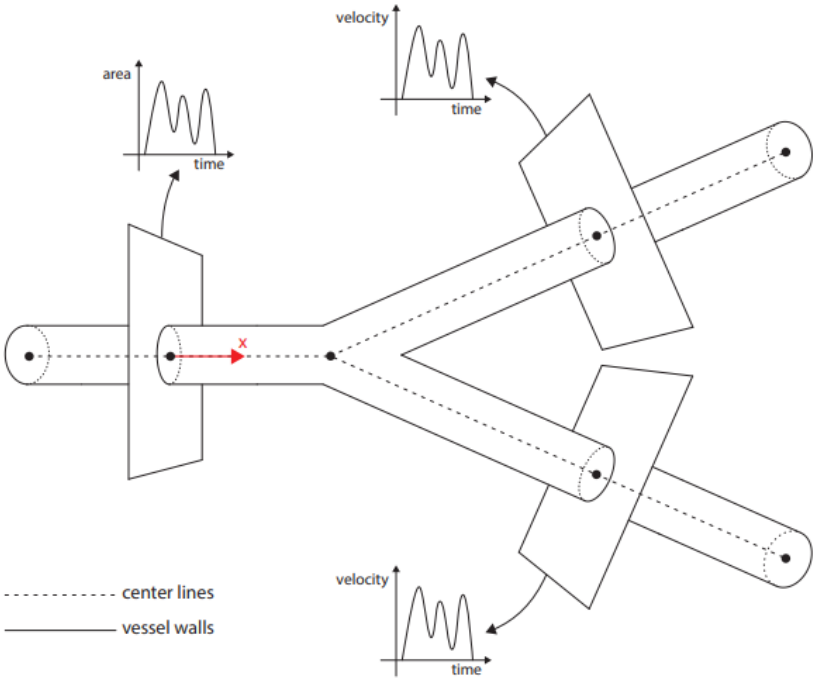

Figure 11. A schematic representation of a simple bifurcating arterial topology

At each point of the junction of the vessels these equations take the form:

$$S_1 v_1 = S_2 v_2 + S_3 v_3$$

$$p_1 + \frac{1}{2}\rho v_1^2 = p_2 + \frac{1}{2}\rho v_2^2$$

$$p_1 + \frac{1}{2}\rho v_1^2 = p_3 + \frac{1}{2}\rho v_3^2,$$

where S - cross-sectional area, v – blood flow rate, p – vessel pressure, ρ – density.

It is necessary to minimize the difference between the left and right parts of the equations (residual), in order for the model result to comply with the laws of hemodynamics. A complete list of the residuals for all 16 vessels of the graph is given in Appendix 1. Moreover, heart and three capillary systems should be considered separately. Since the number of capillaries is too large and there is no need for excessive detail in the graph, it was decided to replace the small capillaries branches with one equivalent branch and consider for them, as well as for the heart, the systolic and diastolic pressure drop (Δp_{heart}, $\Delta p_{capillaries}$) by using the following ratios:

$$p_k + \frac{1}{2}\rho v_k^2 = p_{ij} + \frac{1}{2}\rho v_{ij}^2 + \Delta p_{heart}$$

$$p_{xy} + \frac{1}{2}\rho v_{xy}^2 = p_z + \frac{1}{2}\rho v_z^2 + \Delta p_{capillaries}$$

where ρ – density, p_i – i-th vessel pressure, v_i – i-th vessel blood flow rate.

2.4 Cardiovascular system parameters

The blood system parameters generated by a neural network should not only satisfy the laws of hemodynamics, but also should be close to real physiological characteristics of the human circulatory system. Average statistical values of such characteristics are well known in medical literature [17]. Table 1 shows these characteristics for the simplified graph (the numbering coincides with the numbering of the graph edges).

№	Name	p, mmHg	v, cm/s	S, cm^2	l, cm
0	Aorta	95.7	5.5	2.22	58.5
1	Left common iliac artery	95.7	4.7	1.3	7.5
2	Right common iliac artery	95.7	4.7	1.3	7.5
3	Left femoral artery	94.1-95.7	10.4	0.49	30
4	Left internal iliac artery	94.4	14.75	0.07	4
5	Right femoral artery	94.1-95.7	10.4	0.49	30
6	Right internal iliac artery	94.4	14.75	0.07	4
7	Pelvic arteries	94.1-95.7	10.4	0.195	12
8	Veins of the small pelvis	5.9-7.0	8.2-9.1	0.235	12
9	Left internal iliac vein	5.5	7.35	0.135	7.9
10	Right internal iliac vein	5.5	7.35	0.135	7.9
11	Left femoral vein	5.1-6.5	8.8-10.4	0.49-0.58	30
12	Right femoral vein	5.1-6.5	8.8-10.4	0.49-0.58	30
13	Right common iliac vein	5.1	3.4	1.79	5.2
14	Left common iliac vein	5.1	3.4	1.79	5.2
15	Hollow vein	5.1	3.8	3.16	50

Table 1. Average values of blood flow parameters of a healthy person

2.5 GAN modelling

This paper presents several models based on generative-adversarial networks.

2.5.1 Standard GAN architecture

The standard network-generator and network-discriminator were implemented according to the recommendations [20].

Generator implementation

Scheme of the generator's architecture is shown in the Figure 12.

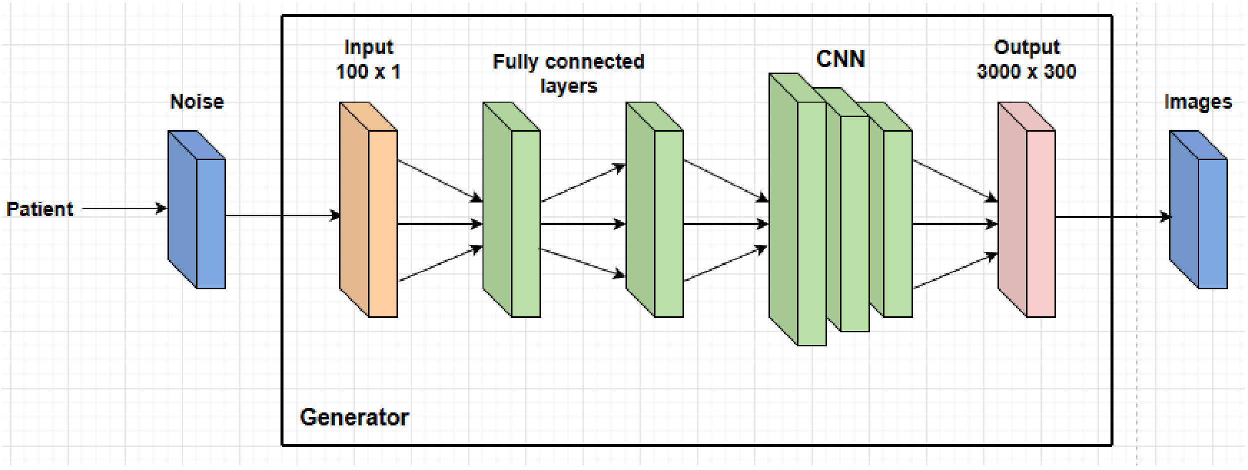

Figure 12. Generator model architecture

The generator input is a vector-noise of dimension 100. Passing through the generator's fully connected layers, it is converted into a 150x15 image. The next layers are the convolution layers, each of which is followed by a batch-normalization layer. The output image size is 3000x300. Below is the developed Python code for generator (Fig. 13):

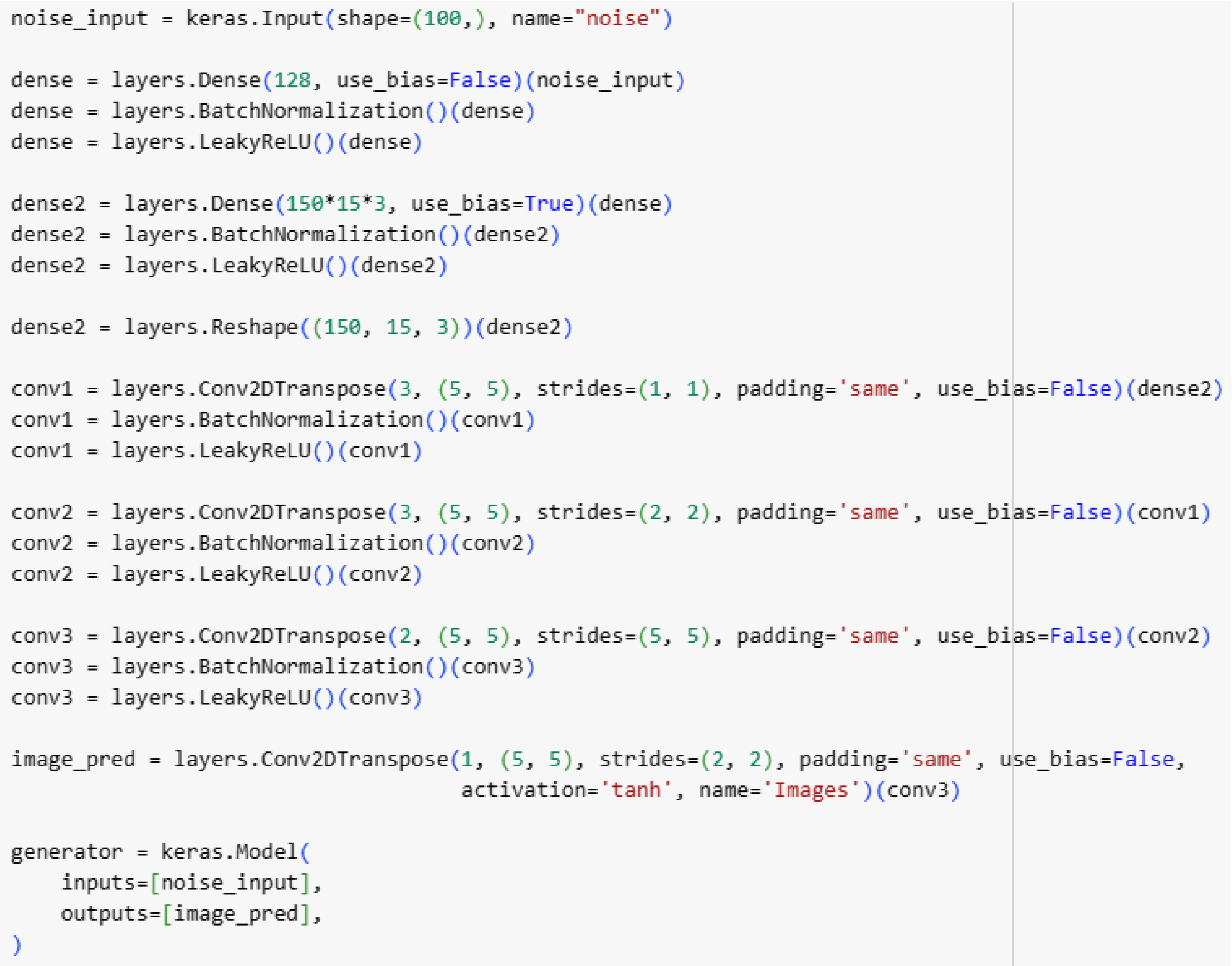

```
noise_input = keras.Input(shape=(100,), name="noise")

dense = layers.Dense(128, use_bias=False)(noise_input)
dense = layers.BatchNormalization()(dense)
dense = layers.LeakyReLU()(dense)

dense2 = layers.Dense(150*15*3, use_bias=True)(dense)
dense2 = layers.BatchNormalization()(dense2)
dense2 = layers.LeakyReLU()(dense2)

dense2 = layers.Reshape((150, 15, 3))(dense2)

conv1 = layers.Conv2DTranspose(3, (5, 5), strides=(1, 1), padding='same', use_bias=False)(dense2)
conv1 = layers.BatchNormalization()(conv1)
conv1 = layers.LeakyReLU()(conv1)

conv2 = layers.Conv2DTranspose(3, (5, 5), strides=(2, 2), padding='same', use_bias=False)(conv1)
conv2 = layers.BatchNormalization()(conv2)
conv2 = layers.LeakyReLU()(conv2)

conv3 = layers.Conv2DTranspose(2, (5, 5), strides=(5, 5), padding='same', use_bias=False)(conv2)
conv3 = layers.BatchNormalization()(conv3)
conv3 = layers.LeakyReLU()(conv3)

image_pred = layers.Conv2DTranspose(1, (5, 5), strides=(2, 2), padding='same', use_bias=False,
                                    activation='tanh', name='Images')(conv3)

generator = keras.Model(
    inputs=[noise_input],
    outputs=[image_pred],
)
```

Figure 13. Developed generator code

Discriminator implementation

Scheme of the discriminator’s architecture is shown in the Figure 14.

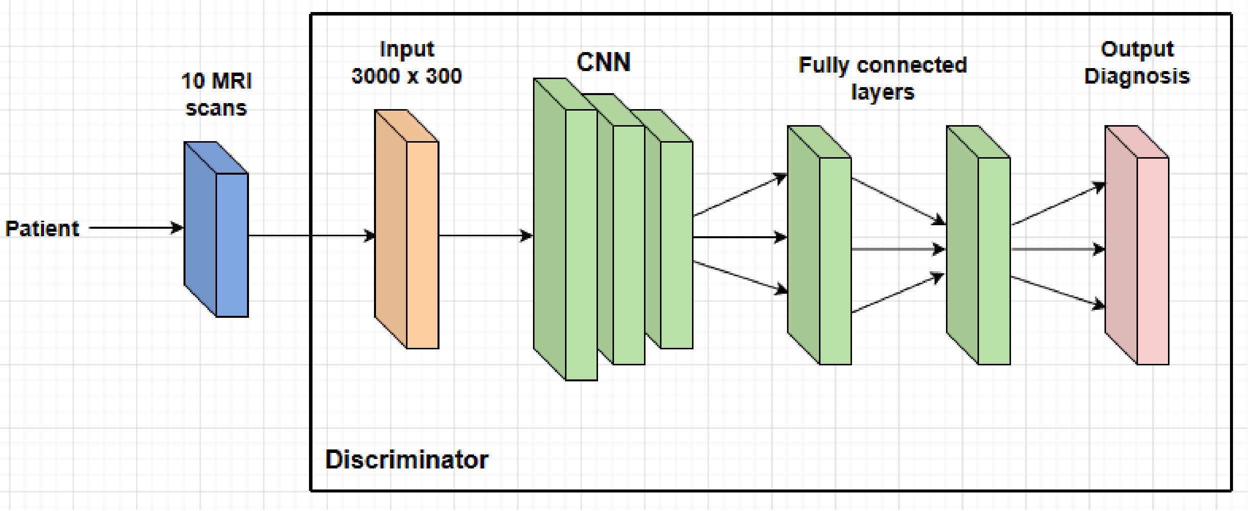

Figure 14. Discriminator model architecture

The discriminator inputs an image of size 3000x300 with 1 channel. Then on each layer the size of images is reduced, and the number of filters is changed. The convolution layer has a size of 750x75 with one filter. Each convolutional layer is followed by batch-normalization layers with LeakyReLU activation function and dropout equal to 0.3 to reduce model overfitting probability. The fully connected layers use the ReLu activation function. The output is a single number determining whether the patient is sick or healthy. Below is the developed Python code for discriminator (Fig. 15):

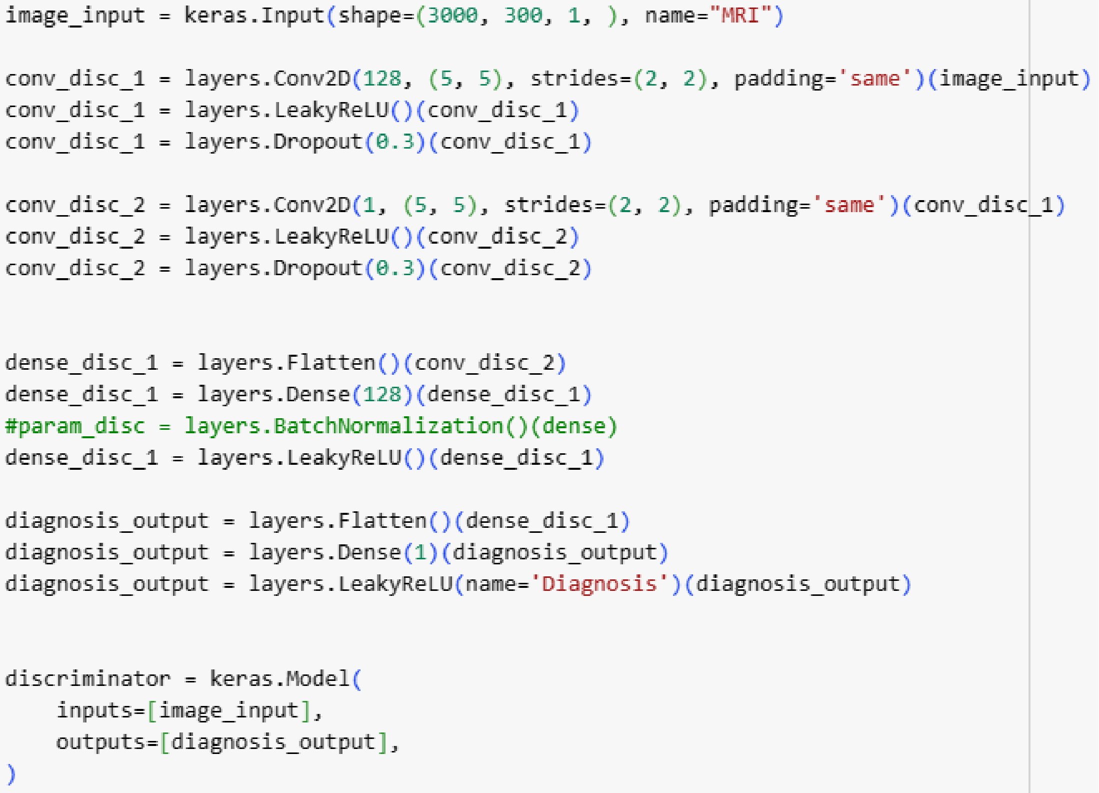

```
image_input = keras.Input(shape=(3000, 300, 1, ), name="MRI")

conv_disc_1 = layers.Conv2D(128, (5, 5), strides=(2, 2), padding='same')(image_input)
conv_disc_1 = layers.LeakyReLU()(conv_disc_1)
conv_disc_1 = layers.Dropout(0.3)(conv_disc_1)

conv_disc_2 = layers.Conv2D(1, (5, 5), strides=(2, 2), padding='same')(conv_disc_1)
conv_disc_2 = layers.LeakyReLU()(conv_disc_2)
conv_disc_2 = layers.Dropout(0.3)(conv_disc_2)


dense_disc_1 = layers.Flatten()(conv_disc_2)
dense_disc_1 = layers.Dense(128)(dense_disc_1)
#param_disc = layers.BatchNormalization()(dense)
dense_disc_1 = layers.LeakyReLU()(dense_disc_1)

diagnosis_output = layers.Flatten()(dense_disc_1)
diagnosis_output = layers.Dense(1)(diagnosis_output)
diagnosis_output = layers.LeakyReLU(name='Diagnosis')(diagnosis_output)


discriminator = keras.Model(
    inputs=[image_input],
    outputs=[diagnosis_output],
)
```

Figure 15. Developed discriminator code

Loss function

Model training takes place by the standard method of error backpropagation using the Adam optimizer with the learning step $\alpha = 1e - 04$, and the binary cross-entropy is used as the loss function:

$$BinaryCrossentropy = -(y \cdot log(p) + (1 - y) \cdot \log(1 - p)),$$

where y is a binary indicator (0 or 1), and p is the predicted probability of belonging to the class. The loss is calculated using TensorFlow functions.

2.5.2 GAN with PINN

Introducing physical information about cardiovascular system using simplified blood system graph involves adding a hidden layer with 50 neurons to the model: each neuron for 3 parameters (velocity, pressure and cross-sectional area) for each of the 16 vessels, and 2 variables Δp_{heart} and $\Delta p_{capillaries}$.

Modifying generator and discriminator

Two blocks should be added to generator and discriminator models, where the first one converts input vector into blood system parameters, and the second one converts parameters into output. Both newly added blocks of the model should be combined into a single network, as it is essential that the second block can affect the weights of the layers of the first block, so that the network generates not only physically realistic parameters, but also different for sick and healthy patients, so that the discriminator is able to distinguish them.

The architecture of the generator and discriminator models remained relatively unchanged compared to the standard GAN model, except adding four new layers (Fig. 16).

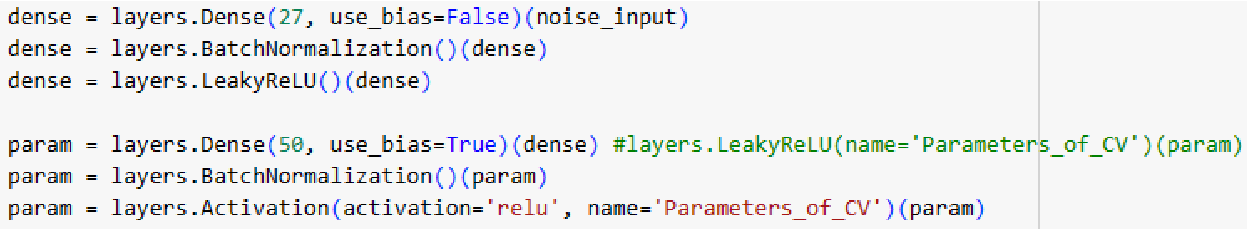

```
dense = layers.Dense(27, use_bias=False)(noise_input)
dense = layers.BatchNormalization()(dense)
dense = layers.LeakyReLU()(dense)

param = layers.Dense(50, use_bias=True)(dense) #layers.LeakyReLU(name='Parameters_of_CV')(param)
param = layers.BatchNormalization()(param)
param = layers.Activation(activation='relu', name='Parameters_of_CV')(param)
```

Figure 16. Added layers

Loss function

In addition to the binary cross-entropy used in standard GAN model, an additional $Loss_{residuals}$ function is introduced, which includes residual approach [19].

$$Loss_{residuals} = \frac{1}{N}\sum_{i=0}^{N}\left(S_0^i v_0^i - \sum_{j=1}^{n_i} S^i{}_j v_j^i\right)^2 + \frac{1}{N}\sum_{i=0}^{N}\left(\sum_{j=1}^{n_i}\left(p_0^i + \frac{1}{2}\rho(v_0^i)^2 - p_j^i - \frac{1}{2}\rho(v_j^i)^2\right)\right)^2$$

$$+\frac{1}{N_{\text{с}}}\sum_{i=N}^{N+N_h}\left(\sum_{j=1}^{n_i}(p_0^i + \frac{1}{2}\rho(v_0^i)^2 - p_j^i - \frac{1}{2}\rho(v_j^i)^2 - \Delta p_{heart})\right)^2$$

$$+\frac{1}{N_{\text{к}}}\sum_{i=N+N_h}^{N+N_h+N_c}\left(\sum_{j=1}^{n_i}(p_0^i + \frac{1}{2}\rho(v_0^i)^2 - p_j^i - \frac{1}{2}\rho(v_j^i)^2 - \Delta p_{capillaries})\right)^2$$

where N_h - number of collocation points with Δp_{heart}, N_c - number of collocation points with $\Delta p_{capillaries}$, N – number of remaining collocation points, n_i – number of edges, $S^i{}_j$, v_j^i, p_j^i – parameters for i-th point.

Minimizing this loss function allows the neural network to generate parameters of the circulatory system that satisfy the laws of hemodynamics, which should improve the efficiency of both the generator and the discriminator. Learning takes place with the simultaneous use of two loss functions. Using the Adam backpropagation optimizer, the model weights errors are corrected in two passes. The first iteration, the binary cross-entropy function is applied and the weights of all layers from first to last are changed according to the value of this function. At the second iteration, according to the value of the $Loss_{residuals}$ function, the weights of only those layers that are responsible for the generation of the cardiovascular parameters are changed.

2.6 Chapter results

This chapter describes architectures and configurations of models based on Generative-Adversarial Networks. Standard GAN model and modified GAN using the PINN paradigm are proposed. It is expected that this approach should improve the quality of the original model by integrating graph of the human cardiovascular system and average blood flow parameters, considering hemodynamics laws. The results of the computational experiment and comparative analysis of the quality of the models described above are provided in the next chapter.

Chapter 3. Computational experiment and results analysis

3.1 Development tools

The code was developed using Python, which has an extensive set of libraries for solving machine learning problems and is the most common programming language in data analysis. Standard libraries scikit-learn and numpy were used for preprocessing of MRI images, and matplotlib for visualization of images and plotting. TensorFlow, Keras, numpy and pandas libraries were used for developing and training the model. Computational experiments were carried out using the Google Colab environment.

3.2 Metrics

The model's performance is assessed based on calculation of the loss function. Moreover, standard metrics Accuracy, Precision, Recall and F1-Score are used to evaluate the accuracy of the discriminator predictions. Precision measures the number of the positive predictions made which are actually correct (true positives). Recall measures how many of the positive cases correctly predicted over all the positive cases in the initial dataset. F1-Score is a measure combining both precision and recall, or more precisely, harmonic mean of the two. The goal is to offer a single metric that equally weighs the precision and recall ratios. [21].

The test sample contains 21 randomly selected MRI images from the initial dataset and 10 generated images. The size of the images is 3000×300 pixels. The generated parameters of the circulatory system are checked for physical plausibility by comparing them with the reference values provided in Table 1. Model training was typically performed up to 500 epochs. After each iteration, metrics were computed, and the quality of the model was checked on a test sample.

3.3 Achieved results

This chapter shows the computational results after model development and training. The focus is on standard generative-adversarial network and its comparison with the same model but using physics-informed layers (PINN paradigm) in accordance with abovementioned human cardiovascular system knowledge.

3.3.1 Standard GAN

The standard GAN model was trained to demonstrate the role of architecture in model efficiency. Below is a graph of discriminator accuracy on the test dataset as a function of the number of epochs (Fig. 17).

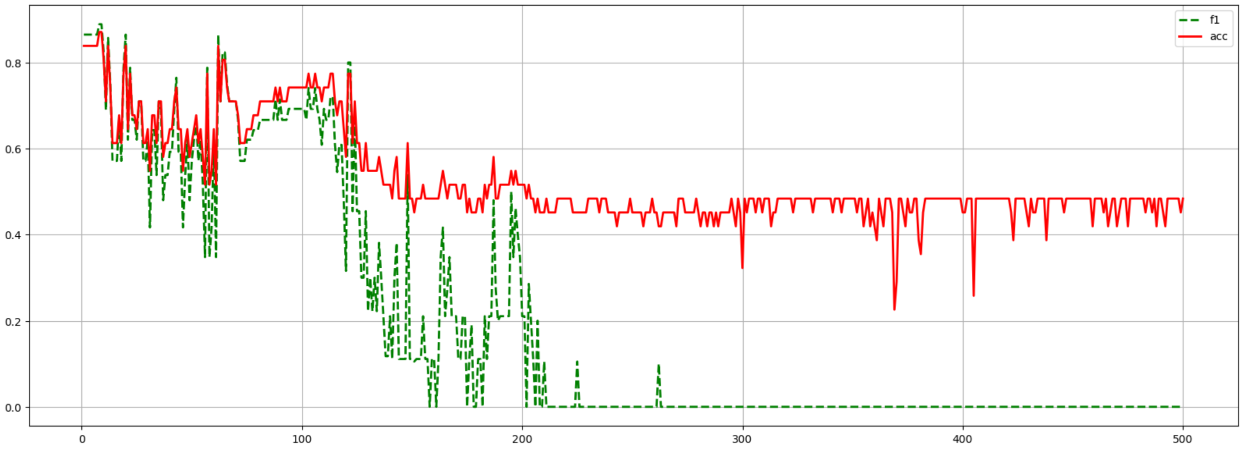

Figure 17. Standard GAN accuracy and F1-score

We can notice that after 200 epochs the accuracy metric decreases significantly and becomes equal to approximately 50%, while F1-score drops down to 0. It may indicate that the model does not work any better than flipping a coin and classifies all patients as healthy due to overfitting. A conclusion can be made that standard generative-adversarial model works best for 100 epochs.

The following graph shows the values of the loss function (BinaryCrossentropy, as noted in Chapter 2) as a function of the number of epochs for the same model (Fig.18).

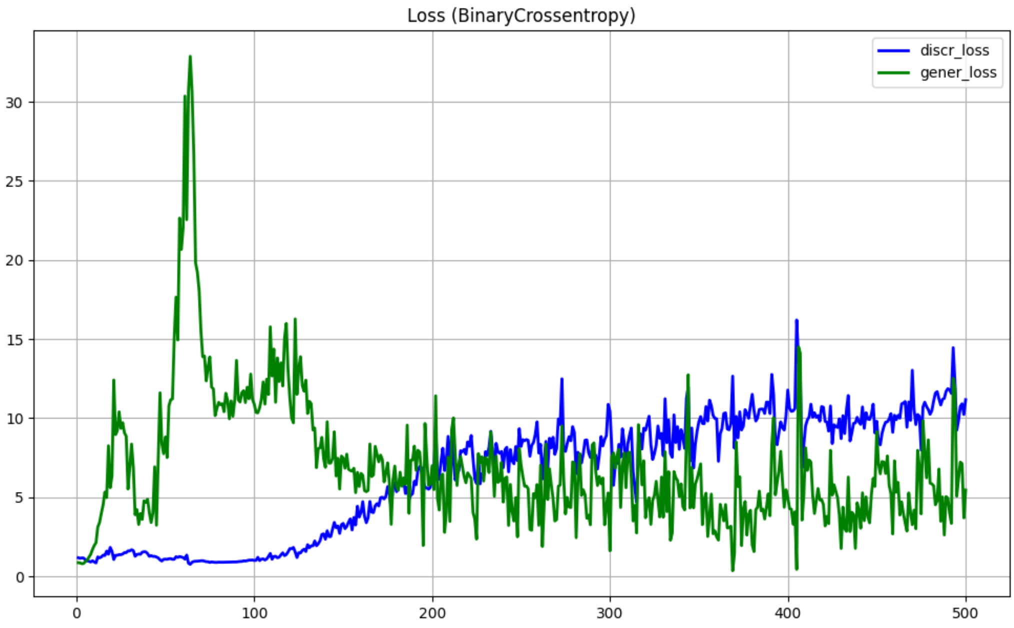

Figure 18. Loss function values for standard GAN

We can notice that the graph becomes smoother, and from about the 200th epoch the values of the generator and discriminator loss functions start to converge. In turn, the model training process is relatively unstable, as there are several outliers which can be clearly spotted.

As for generated images, in the Figure 19 there are samples taken on the epoch 500. First two rows belong to one patient, next two rows belong to the second patient, and the last two rows in the image belong to the third patient respectively.

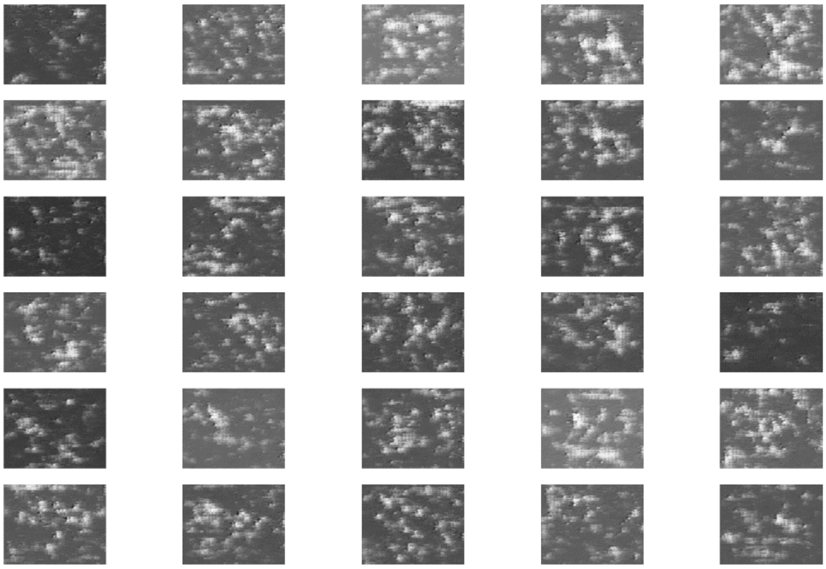

Figure 19. Standard GAN generated images

The images generated by this model are of very low quality, even though they still look like MRI images. This could happen due to mistakes made in the process of modelling generator, wrong instructions for discriminator, or lack of sufficient information. The last reason we are going to test further, adding physics-informed neural layers.

3.3.2 GAN with PINN

Physics-informed neural network paradigm was introduced to evaluate the effect of information about the laws of hemodynamics on the quality of the model. Below is a graph of discriminator accuracy on the test dataset as a function of the number of epochs (Fig. 20).

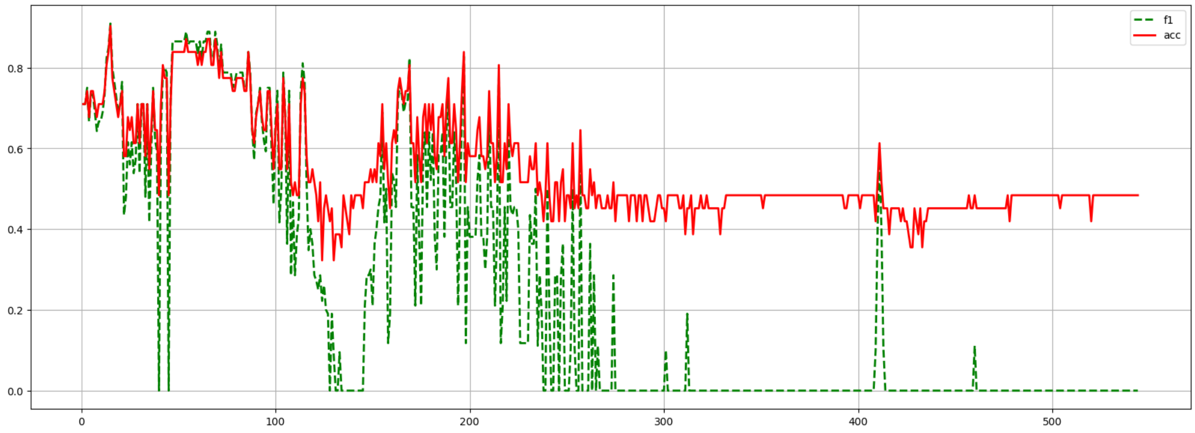

Figure 20. GAN with PINN accuracy and F1-score

There was no significant improvement in the quality of the model compared to the model from the previous point. The process of overfitting could be noticed again, but for now starting from 300th epoch.

As for loss functions, in this case together with the standard binary cross-entropy approach we also consider a new residuals loss function, introduced in paragraph 2.5.2 (Fig. 21).

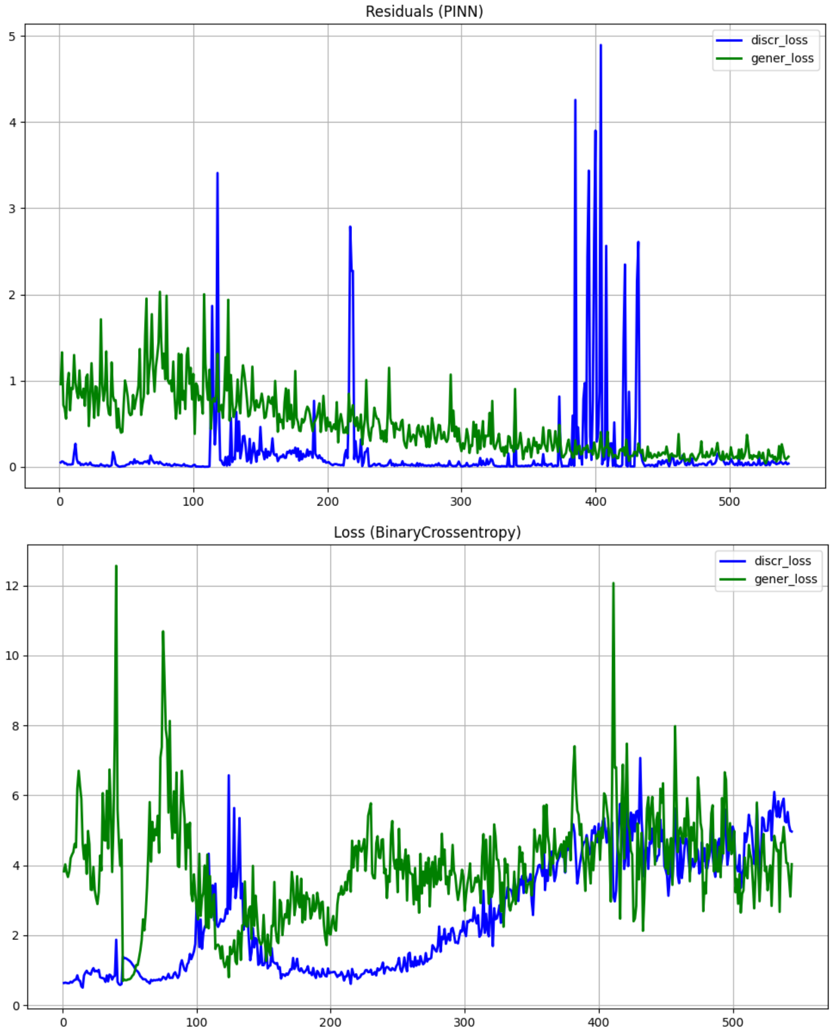

Figure 21. Loss function values for GAN with PINN

Even though residuals loss function gives some outliers for discriminator, it converges up to 500th epoch and almost reaches 0. In turn, binary cross-entropy loss function results could be compared with the graph for the standard GAN model (Fig. 18). Here we can notice a great results improvement, as the graph became a lot smoother, and the loss value decreased by 2 times for both generator and discriminator.

Generated images quality remains low, nevertheless they look different from those provided for standard GAN (Fig. 22). The reason for this is the above-mentioned principle of discriminator, which considers images of sick patients as "real", and images of healthy and generated - as "generated". As a result, during the first iterations of training, the discriminator assigns to the same class both images of healthy people and noise, from which the generator is unable to generate high-quality images.

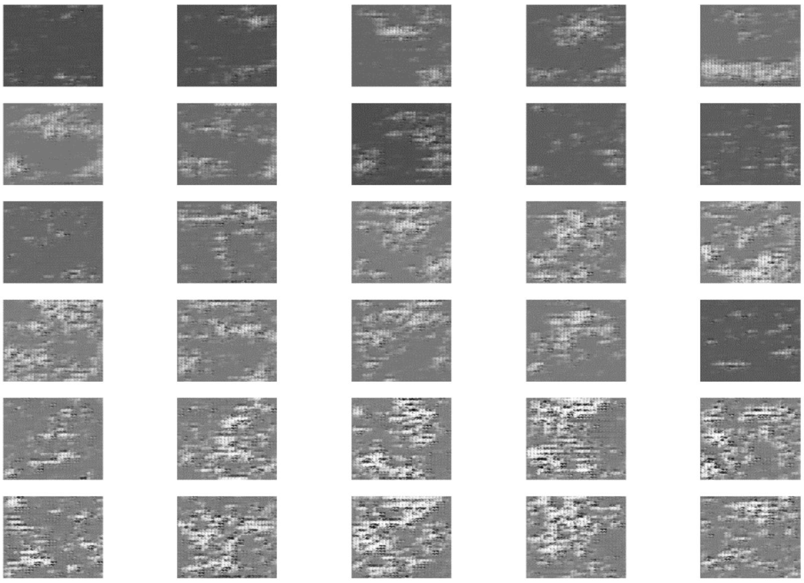

Figure 22. GAN with PINN generated images

Blood flow parameters generated by the model are far from real parameters provided in the Table 1, as all of them are close to 0.

3.4 Conclusion on the results

All the models described in Chapter 2 have been implemented and their quality has been compared. The hypothesis about the efficiency of using the PINN paradigm in combination with GAN is confirmed, however accuracy of the model is still low, its weaknesses have been identified, so the directions of further work became known.

Conclusion

During the work on thesis paper a number of tasks were accomplished. In particular, cardiovascular system and human hemodynamics have been studied through a literature review, leading to presented cardiovascular graph and mathematical equations derived from hemodynamics laws. The next step was to perform dataset analysis and preprocessing. MRI images were cropped and transformed to fit in the model in the most effective way. The problem of small and unbalanced dataset was observed, so the solution of using augmentation methods was proposed, namely generative-adversarial networks. Finally, implementation of deep learning neural network step consisted of studying various neural network architectures and developing standard GAN as well as modified GAN using PINN paradigm. The computational experiment was performed, and quality of proposed models was evaluated through various metrics, which gave insights on impact of introducing knowledge about human cardiovascular system to the model. A comparative analysis led to suggestions for further work and model improvement. Thus, in general, the results of the study can be considered successful.

As a result of the thesis paper, it was shown that the use of the PINN paradigm improves the quality of the standard GAN model in generating images and resolving phlebology problem. However, there are still some disadvantages in the model, which should be solved by further modifications. First of all, generated cardiovascular parameters should be limited in specified intervals by implementing tools such as sigmoid function, for example. At the same time, full CV graph instead of simplified one could give a significant increase in model’s accuracy. Moreover, transfer learning approach should solve the problem of generating low quality images and consequently improve the whole model. Also, some other variants of loss functions might be useful in our case.

Bibliography

1. *Cardiovascular diseases (cvds) World Health Organization*. Available at: https://www.who.int/news-room/fact-sheets/detail/cardiovascular-diseases-(cvds) (Accessed: 29 May 2023).
2. *Статистика сердечно-сосудистых заболеваний в россии, Статистика сердечно сосудистых заболеваний России*. Available at: https://chekhovsc.ru/blog/statistika-serdechno-sosudistykh-zabolevanij-v-rossii (Accessed: 29 May 2023).
3. Tan, W. *et al.* (2023) ‘Bayesian inference and dynamic neural feedback promote the clinical application of intelligent congenital heart disease diagnosis’, *Engineering* [Preprint]. doi:10.1016/j.eng.2022.10.015.
4. Moazemi, S. *et al.* (2023) ‘Artificial Intelligence for clinical decision support for monitoring patients in CARDIOVASCULAR ICUS: A systematic review’, *Frontiers in Medicine*, 10. doi:10.3389/fmed.2023.1109411.
5. Tang, R. *et al.* (2022) ‘Artificial Intelligence in intensive care medicine: Bibliometric analysis’, *Journal of Medical Internet Research*, 24(11). doi:10.2196/42185.
6. Larentzakis, A. and Lygeros, N. (2021a) ‘Artificial Intelligence (AI) in medicine as a strategic valuable tool’, *Pan African Medical Journal*, 38. doi:10.11604/pamj.2021.38.184.28197.
7. Anton, N. *et al.* (2022) ‘Comprehensive review on the use of Artificial Intelligence in Ophthalmology and Future Research Directions’, *Diagnostics*, 13(1), p. 100. doi:10.3390/diagnostics13010100.
8. Dhar, T. *et al.* (2023) ‘Challenges of deep learning in medical image analysis—improving explainability and Trust’, *IEEE Transactions on Technology and Society*, 4(1), pp. 68–75. doi:10.1109/tts.2023.3234203.
9. Zhou, T. *et al.* (2023) ‘Deep Learning Methods for Medical Image Fusion: A Review’, *Computers in Biology and Medicine*, 160, p. 106959. doi:10.1016/j.compbiomed.2023.106959.
10. Kshatri, S.S. and Singh, D. (2023) ‘Convolutional neural network in Medical Image Analysis: A Review’, *Archives of Computational Methods in Engineering*, 30(4), pp. 2793–2810. doi:10.1007/s11831-023-09898-w.
11. Gogineni, R. and Chaturvedi, A. (2022) ‘Convolutional Neural Networks for medical image analysis’, *Convolutional Neural Networks for Medical Image Processing Applications*, pp. 75–90. doi:10.1201/9781003215141-4.

12. *Cutting-splicing data augmentation: A novel technology for medical ...* Available at: https://www.researchgate.net/publication/364438788_Cutting-Splicing_data_augmentation_A_novel_technology_for_medical_image_segmentation/fulltext/63517b1d96e83c26eb3aeaed/Cutting-Splicing-data-augmentation-A-novel-technology-for-medical-image-segmentation.pdf (Accessed: 29 May 2023).
13. Armanious, K. *et al.* (2020) ‘Medgan: Medical image translation using gans’, *Computerized Medical Imaging and Graphics*, 79, p. 101684. doi:10.1016/j.compmedimag.2019.101684.
14. Sarabian, M., Babaee, H. and Laksari, K. (2022) ‘Physics-informed neural networks for brain hemodynamic predictions using medical imaging’, *IEEE Transactions on Medical Imaging*, 41(9), pp. 2285–2303. doi:10.1109/tmi.2022.3161653.
15. V.B. Koshelev, S.I. Mukhin, N.V. Sosnin, A.P. Favorsky (2010) *Mathematical models of quasi-uniform hemodynamics*: Manual. - M.MAKS Press, 114 pp.
16. Bunicheva, A.Ya. *et al.* (2015) ‘Mathematical modeling of quasi-one-dimensional hemodynamics’, *Computational Mathematics and Mathematical Physics*, 55(8), pp. 1381–1392. doi:10.1134/s0965542515080060.
17. Vassilevski, Y. *et al.* (2020) *Personalized computational hemodynamics: Models, methods, and applications for vascular surgery and Antitumor Therapy*. London: Academic Press.
18. *CEAP classification of venous disorders - statpearls - NCBI bookshelf*. Available at: https://www.ncbi.nlm.nih.gov/books/NBK557410/ (Accessed: 29 May 2023).
19. Kissas, G. *et al.* (2020) ‘Machine learning in Cardiovascular flows modeling: Predicting arterial blood pressure from non-invasive 4D flow MRI data using physics-informed Neural Networks’, *Computer Methods in Applied Mechanics and Engineering*, 358, p. 112623. doi:10.1016/j.cma.2019.112623.
20. Chen, Y. *et al.* (2022) ‘Generative adversarial networks in Medical Image Augmentation: A Review’, *Computers in Biology and Medicine*, 144, p. 105382. doi:10.1016/j.compbiomed.2022.105382.
21. Kanstrén, T. (2021) *A look at precision, recall, and F1-score, Medium*. Available at: https://towardsdatascience.com/a-look-at-precision-recall-and-f1-score-36b5fd0dd3ec (Accessed: 30 May 2023).
22. Semekovich T. (2022) *Phlebology Disease Classification Based on Deep Learning Neural Networks*
23. Aljawarneh, S. *et al.* (2019) *Particularities of data mining in medicine: Lessons learned from Patient Medical Time Series Data Analysis - EURASIP Journal on Wireless*

Communications and networking, *SpringerOpen*. Available at: https://jwcn-eurasipjournals.springeropen.com/articles/10.1186/s13638-019-1582-2 (Accessed: 30 May 2023).

24. Uchida, S. (2013) ‘Image processing and recognition for biological images’, *Development, Growth & Differentiation*, 55(4), pp. 523–549. doi:10.1111/dgd.12054.
25. Ren, H. (2023) ‘Optimization of lung CT image processing and recognition based on E-SRG segmentation algorithm’, *BIO Web of Conferences*, 59, p. 03002. doi:10.1051/bioconf/20235903002.
26. Zhou, C., Zhang, Y. and Yang, L. (2021) ‘Medical image recognition based on improved convolutional neural network’, *Lecture Notes in Electrical Engineering*, pp. 204–212. doi:10.1007/978-981-33-6318-2_26.

Appendix 1

List of residuals:

0 = 1 + 2	$A_0u_0 - A_1u_1 - A_2u_2$ $p_0 + \frac{1}{2}\rho u_0^2 - p_1 - \frac{1}{2}\rho u_1^2$ $p_0 + \frac{1}{2}\rho u_0^2 - p_2 - \frac{1}{2}\rho u_2^2$
1 = 3 + 4	$A_1u_1 - A_3u_3 - A_4u_4$ $p_1 + \frac{1}{2}\rho u_1^2 - p_3 - \frac{1}{2}\rho u_3^2$ $p_1 + \frac{1}{2}\rho u_1^2 - p_4 - \frac{1}{2}\rho u_4^2$
2 = 5 + 6	$A_2u_2 - A_5u_5 - A_6u_6$ $p_2 + \frac{1}{2}\rho u_2^2 - p_5 - \frac{1}{2}\rho u_5^2$ $p_2 + \frac{1}{2}\rho u_2^2 - p_6 - \frac{1}{2}\rho u_6^2$
7 = 4 + 6	$A_7u_7 - A_4u_4 - A_6u_6$ $p_7 + \frac{1}{2}\rho u_7^2 - p_4 - \frac{1}{2}\rho u_4^2$ $p_7 + \frac{1}{2}\rho u_7^2 - p_6 - \frac{1}{2}\rho u_6^2$
3 = 12	$A_3u_3 - A_{12}u_{12};\ p_{12} + \frac{1}{2}\rho u_{12}^2 - p_3 - \frac{1}{2}\rho u_3^2 - \Delta p_{cappilaries}$
5 = 11	$A_5u_5 - A_{11}u_{11};\ p_{11} + \frac{1}{2}\rho u_{11}^2 - p_5 - \frac{1}{2}\rho u_5^2 - \Delta p_{cappilaries}$
7 = 8	$A_7u_7 - A_8u_8;\ p_8 + \frac{1}{2}\rho u_8^2 - p_7 - \frac{1}{2}\rho u_7^2 - \Delta p_{cappilaries}$
8 = 9 + 10	$A_8u_8 - A_9u_9 - A_{10}u_{10}$ $p_8 + \frac{1}{2}\rho u_8^2 - p_9 - \frac{1}{2}\rho u_9^2$ $p_8 + \frac{1}{2}\rho u_8^2 - p_{10} - \frac{1}{2}\rho u_{10}^2$
13 = 10 + 11	$A_{13}u_{13} - A_{10}u_{10} - A_{11}u_{11}$ $p_{13} + \frac{1}{2}\rho u_{13}^2 - p_{10} - \frac{1}{2}\rho u_{10}^2$ $p_{13} + \frac{1}{2}\rho u_{13}^2 - p_{11} - \frac{1}{2}\rho u_{11}^2$
14 = 12 + 9	$A_{14}u_{14} - A_{12}u_{12} - A_9u_9$ $p_{14} + \frac{1}{2}\rho u_{14}^2 - p_{12} - \frac{1}{2}\rho u_{12}^2$ $p_{14} + \frac{1}{2}\rho u_{14}^2 - p_9 - \frac{1}{2}\rho u_9^2$
15 = 13 + 14	$A_{15}u_{15} - A_{13}u_{13} - A_{14}u_{14}$ $p_{15} + \frac{1}{2}\rho u_{15}^2 - p_{13} - \frac{1}{2}\rho u_{13}^2$ $p_{15} + \frac{1}{2}\rho u_{15}^2 - p_{14} - \frac{1}{2}\rho u_{14}^2$
0 = 15	$A_0u_0 - A_{15}u_{15};\ p_0 + \frac{1}{2}\rho u_0^2 - p_{15} - \frac{1}{2}\rho u_{15}^2 - \Delta p_{heart}$

Appendix 2

GitHub repository link:

arsruts/ThesisWork2023 (github.com)